Smart Structures and Systems, *Vol. 29, No. 3 (2022) 421-431*
https://doi.org/10.12989/sss.2022.29.3.421

Crack detection in concrete slabs by graph-based anomalies calculation

Weifang Sun [1], Yuqing Zhou*[1], Jiawei Xiang [1], Binqiang Chen [2] and Wei Feng [3]

[1] *College of Mechanical and Electrical Engineering, Wenzhou University, Wenzhou 325035, China*
[2] *School of Aerospace Engineering, Xiamen University, Xiamen 361005, China*
[3] *College of Mechanical and Electrical Engineering, Henan University of Technology, Zhengzhou 450001, China*

(*Received November 12, 2020, Revised December 13, 2021, Accepted December 17, 2021*)

Abstract. Concrete slab cracks monitoring of modern high-speed railway is important for safety and reliability of train operation, to prevent catastrophic failure, and to reduce maintenance costs. This paper proposes a curvature filtering improved crack detection method in concrete slabs of high-speed railway via graph-based anomalies calculation. Firstly, large curvature information contained in the images is extracted for the crack identification based on an improved curvature filtering method. Secondly, a graph-based model is developed for the image sub-blocks anomalies calculation where the baseline of the sub-blocks is acquired by crack-free samples. Once the anomaly is large than the acquired baseline, the sub-block is considered as crack-contained block. The experimental results indicate that the proposed method performs better than convolutional neural network method even under different curvature structures and illumination conditions. This work therefore provides a useful tool for concrete slabs crack detection and is broadly applicable to variety of infrastructure systems.

Keywords: anomalies evaluation; concrete slabs; crack detection; high-speed railway

1. Introduction

As one of the most popular, providing comfortable, fast, punctual, and convenient transport services, high-speed railway (HSR) has become an essential pillar of China's transportation network (Wang *et al*. 2016). The Chinese HSR network transports dramatic amounts of passengers with 1.7 billion trips in 2017 (Li *et al*. 2019). Therefore, accurate state evaluation and periodic maintenance are crucial for HSR running safety, to prevent catastrophic failure. Nowadays, the maintenance operations of the HSR are typically taking place during nighttime (Fan *et al*. 2018), while thousands of kilometers of HSR network have to suspended to ensure the safety of engineers. With the increase of labor costs in China and the requirement of reliable inspection, traditional large-scale manual detection methods are facing challenges and it is worthwhile devoting much effort to this. Therefore, automatic HSR monitoring has become an important research direction.

Instead of the sleepers in traditional tracks (Fig. 1(b)), concrete slabs are widely used in HSR (Fig. 1(a)) because it considerably requires less maintenance and offers a longer service life and reduced life-cycle costs (Colla *et al*. 2002). Being an important supporting componence, concrete slabs play an important role in HSR's reliable operation. However, generating alternating impacts during the serving period (as fast as 350 km/h), as well as the extreme weather conditions, will inevitably accelerate the slabs deterioration and leads to the generation of cracks (Ai *et al*. 2018). Regular inspection of cracks offers a reliable evaluation for HSR concrete slabs. Although China Academy of Railway Science has developed two major automated inspection trains, the identification of the slabs still relies on the manual review of the track imagery (Ai *et al*. 2018). The skill level and experience of the inspectors will extremely influence the diagnosis accuracy, therefore, accurate complete manual review for thousand kilometers of HSR network during the nighttime seems nearly impossible.

To address the limitations of manual review of visual inspection, considerable efforts have been devoted to the automatic crack detection; the measurement techniques include laser displacement sensors, accelerometers, acoustic emission sensors, and ultrasound imaging methods. Based on the triangulation principle, the height profile of various target surfaces can be acquired across the laser displacement sensors, as well as the crack features (Sanchez *et al*. 2013). Existence cracks also have some effect on natural frequencies of the object; therefore, accelerometers have the potential for cracks detection (Xiang *et al*. 2014, Bilge *et al*. 2019). Similarly, acoustic emission also correlated to the crack growth behaviors which can be utilized for structural health monitoring (Leaman *et al*. 2020). Literature also demonstrated that extracted ultrasonic echo signals in the ultrasound imaging method can be used to crack detection (Song and Ni 2018). However, it is reported that the operating cost of these sensors is high. Because of the high cost of sensors and related equipment, in some cases, there are only partially inspected and only for a limited period (Woo and Yeo 2016).

The advent of computer vision methods over the past decade has shown remarkable advantages over the other sensor-based methods such as low cost and low power

*Corresponding author, Ph.D., Associate Professor,
E-mail: zhouyq@wzu.edu.cn

ISSN: 1738-1584 (Print), 1738-1991 (Online)

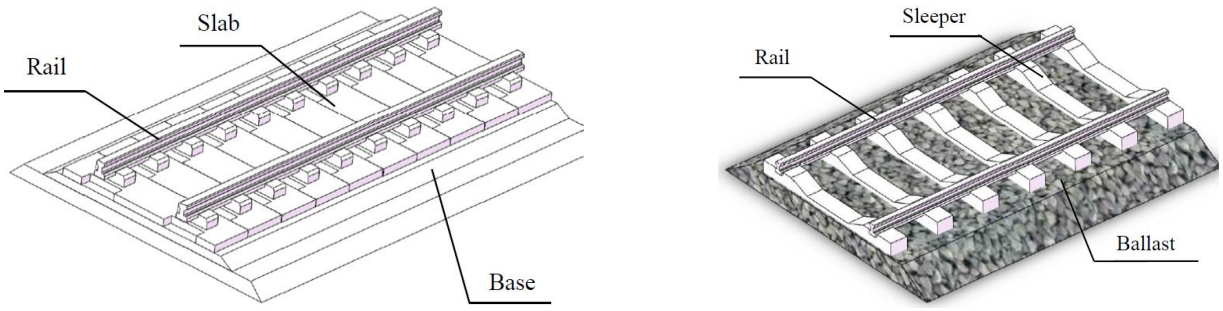

(a) (b)

Fig. 1 Track structures: (a) HSR; (b) conventional train

consumption. There are many excellent reviews in the literature during with infrastructure cracks detection (Xi *et al*. 2018, Ye *et al*. 2019). Bang *et al*. (2019) proposed a novel method for crack detection via salient structure extraction from the textured background, the spatial distribution of texture features is estimated to detect cracks as salient structures that are not widely spread across the whole image. By employing a region-based active contour framework with the intensity cluster energy, Ai *et al*. (2018) investigated a crack identification of HSR slab and identifies more than 93.0% in different crack patterns and complex backgrounds. By introducing a new crack width definition and describing the crack width using the Laplace's Equation, Wang *et al*. (2018) introduced a novel automatic measurement method for pavement crack detection and demonstrated by experimental test. With the improvement of vision equipment, Kong and Li (2019) established a non-contact approach for civil infrastructure breathing crack detection through images overlapping based on the small cyclic movement of the crack path under repetitive fatigue loads and validated through two experiments (small-scale steel compact specimen experiment and large-scale bridge cross-frame connection specimen experiment). However, these computer vision techniques still remain uncertainty because the acquired images are taken under extensively varying real-world situations (Liu *et al*. 2019).

To further improve the efficiency and robustness of the computer vision methods, many machine learning techniques are applied for crack detection. Although exact crack detections are generally difficult, they are obtainable by some types of machine learning techniques. The first type is the convolutional neural network (CNN) and received widely concerns because of the good hierarchical feature representation ability from a lower level to a higher level (Luo *et al*. 2019). Based on CNN, many methods have been investigated in several studies. The existence of deeper network structures, however, needs long computational training time, which makes it more difficult for real implementation scenarios (Nayyeri *et al*. 2019). The second type is the recurrent neural network (RNN), which can address the flow of internal memory and process arbitrary input sequences, and successfully implemented in pavement crack detection (Zhang *et al*. 2019). The third type is the sparse coding. A typical example of sparse coding is a convolutional sparse coding-based deep random vector functional link network proposed by Maeda *et al*. (2019), which can be used for distress classification of road structures. The fourth type is the ensemble learning method, which collects multiple individual classifiers (i.e. learning vector quantization (Bayar and Bilir 2019), random forest classifier (Ozcan *et al*. 2017) and collects decisions of all classifiers to make a final decision (Zhuang *et al*. 2018). However, the previous machine learning techniques require large amounts of training database for robust results (Cha *et al*. 2018). The contained strong noises caused by complex curvature structures and illumination conditions in acquired images of HSR concrete slabs potentially trigger false alarms. Caused by the lack of enough abnormal samples, the generalization ability towards HSR crack detection still strongly influenced by the data size and sample distribution. Therefore, it stills an open challenge for crack detection in practical engineering application scenarios (Kang *et al*. 2018).

Quantitative evaluation of anomalous value from the reference signal is significant for robust state identification in few-shot or zero-shot situations. The visibility graph is an efficient utensil to mapping a time series into a graph (Ahmadlou and Adeli 2012) and received widely concerns (Ahmadlou and Adeli 2017). By establishing the graph structure of time-series, a graph-based change-point detection method has been developed for machine monitoring and successfully verified in real scenarios (Lu *et al*. 2018). Referenced by the basic concepts of the graph in the data structure, the likelihood of potential changes can be investigated according to the graph similarity evaluation (Sun *et al*. 2020). Compared with traditional methods, the graph-based method is more effective for early fault detection in one-dimensional time-domain signals (Wang *et al*. 2019). Various noise interferences are also taking into account the graph-based model which means better robustness in real application scenarios.

Inspired by the idea of graph-based method, authors present a curvature filtering improved non-contact detection method using the captured images for zero-shot cracks detection in HSR concrete slabs. Contained crack information is extracted from the large curvature information contained in acquired images. After that, image sub-blocks anomalies are calculated from the graph Frobenius norm where the baseline of the sub-blocks is acquired by crack-free samples.

The major contributions of this research are summarized

below.

(1) A zero-shot method is proposed for the crack detection of HSR concrete slabs via graph-based anomalies calculation. Compared with other detection methods, the proposed method can recognize the crack samples with few or even no training samples.
(2) A curvature-based crack information extraction approach is proposed for the edge information preservation. Compared with traditional edge detectors, this approach can efficiently magnify the crack features with high robustness.
(3) An image graph structure is established for sub-blocks anomalies calculation. With this structure, the crack features can be identified with high sensitivity, even for slight crack images.

The rest of the paper is organized as follows. The curvature filtering, as well as the graph-based change-point detection method, are briefly described in Section 2. The framework of the proposed method is explained in detail in Section 3. The experimental investigations are shown in Section 4. A comparative analysis of different edge detectors is discussed in Section 5. Some concluding remarks are given in Section 6.

2. The proposed crack detection method

2.1 Overview

To realize the zero-shot crack detection for concrete slabs in HSR, a graph-based anomalies calculation method is developed. The schematic of the curvature filtering improved method is presented in Fig. 2, where the crack features are magnified through a fine-tuning curvature filtering approach (image preprocessing), image sub-blocks anomalies are calculated according to the graph Frobenius norm.

2.2 Curvature filtering

As presented before, acquired images may contain strong noises caused by complex curvature structures and illumination conditions which potentially trigger false alarms in the crack detection. Considering the intensities of the pixels as the height information of curved surfaces, the curvature information of an image can be calculated. This curvature might have the potential to identify the discontinuous changes in image grayscale information. Recently, Gong and Sbalzarini (2017) proposed a curvature filtering method which can be utilized to implicit optimize curvature according to the discrete characteristics of the image without direct curvature calculation. In this section, a fine-tuning curvature filtering approach is proposed to magnify the crack features.

2.2.1 Curvature smoothing

Gong and Sbalzarini (2017) defined the eight directional curvatures (DCs) through arbitrary pixel points (black point in Fig. 3), where two DCs represent the horizontal and vertical directions (Fig. 3(a)), two DCs represent the directions inclined at by 45° and 135° (Fig. 3(b)), and the remaining four DCs represent four triangular regions that do not pass through the center point (Fig. 3(c)).

The geometric relation between the central pixel (black point in Fig. 3) and its two adjacent points along the eight curvature directions can be summarized as two following situations: Figs. 4(a) and (b), where the vertical axis indicates the pixel intensity, $x1$, $x2$, and $x3$ are the adjacent three pixels in an image, R is the curvature radius, d_i is the vertical distance between the middle pixel and the straight line between two adjacent points which marked with a circle, h is the pixel distance.

Assuming the pixel distance is 1, $\alpha \in (0.5\pi\text{-}0.3, 0.5\pi\text{-}0.3)$, the corresponding relationship between curvature and the distance d_i is shown in Fig. 5(a), where the horizontal axis indicates the distance d_i, the vertical axis indicates the curvature, the color bar represents the different α angle. As

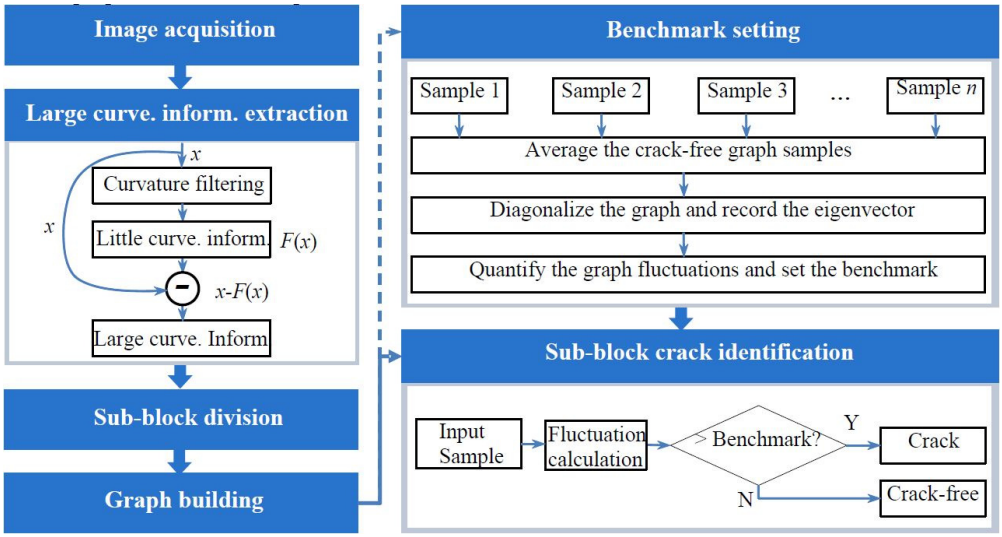

Fig. 2 Flow-chart of the proposed zero-shot crack detection method

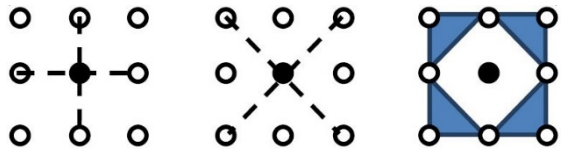

(a) (b) (c)

Fig. 3 Directional curvatures (a) horizontal and vertical directions; (b) directions inclined at by 45° and 135°; (c) four to the tangent planes through mixed neighbors

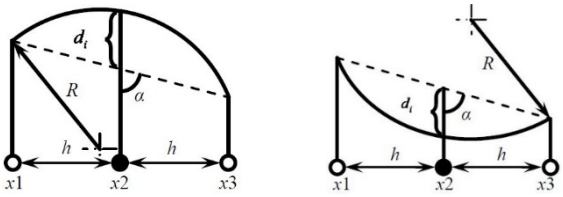

(a) (b)

Fig. 4 Geometric description for directional curvatures: (a) convex; (b) concave

can be seen in Fig. 5, the curvature can be simplified to a linear function. The error caused by this linearization is shown in Fig. 5(b), in which the x-axis represents the distance d_i, the y-axis represents the α angle, and the z-axis is the corresponding curvature error. Even though this approximation is not that accurate, however, it extremely improves the computational complexity (Gong and Sbalzarini 2017), the unpredictable noise generated caused gradient change during the photographing process can also be processed.

Accordingly, the eight directional curvature can be represented as below, where the center pixel coordinate is (i, j), U is the corresponding pixel intensity.

$$\begin{cases} d_1 = (U(i-1,j) + U(i+1,j))/2 - U(i,j) \\ d_2 = (U(i,j\text{-}1) + U(i,j\text{+}1))/2 - U(i,j) \\ d_3 = (U(i-1,j\text{-}1) + U(i+1,j\text{+}1))/2 - U(i,j) \\ d_4 = (U(i-1,j\text{+}1) + U(i+1,j\text{-}1))/2 - U(i,j) \\ d_5 = U(i-1,j) + U(i,j-1) - U(i-1,j-1) - U(i,j) \\ d_6 = U(i-1,j) + U(i,j+1) - U(i-1,j+1) - U(i,j) \\ d_7 = U(i,j-1) + U(i+1,j) - U(i+1,j-1) - U(i,j) \\ d_8 = U(i,j+1) + U(i+1,j) - U(i+1,j+1) - U(i,j) \end{cases} \tag{1}$$

After computing all the directional curvature, we can use the directional curvature to implicit optimize the mean curvature. More specifically, the discrete approximation of the minimal absolute principle curvature on the pixel grid can be described as $|d_m| = min\{|d_i|, i = 1, \ldots, 8\}$. Therefore, the iterative optimization algorithm can be summarized as $\hat{U}(x) = U(x) + d_m$, where $\hat{U}(x)$ is the iterative intermediate image.

2.2.2 Large curvature information extraction

In slabs images, cracks can be seen as sudden changes in the grayscale of the image. Therefore, the large curvature information of the image can reflect the degree of crack to a certain extent. With a shortcut connection, residual network (ResNet) received widely concert because of its high classification accuracy. Inspirited by ResNet, this section proposed a fine-tuning curvature filtering approach to magnify the crack features, where a shortcut connection is employed for the large curvature information extraction.

The fundamental structure of the proposed approach is shown in Fig. 1. Assuming the input raw image is x, the curvature filtering function is F, the output vector y, can be represented as

$$y = x - F(x) \tag{2}$$

As discussed before, low curvature filtering componence $F(x)$ can be received after the curvature filtering process. Therefore, the high curvature componence y can be inferred from Eq. (2). The follow-up experiments also demonstrate this high curvature componence contains many crack features which can be used for the detection.

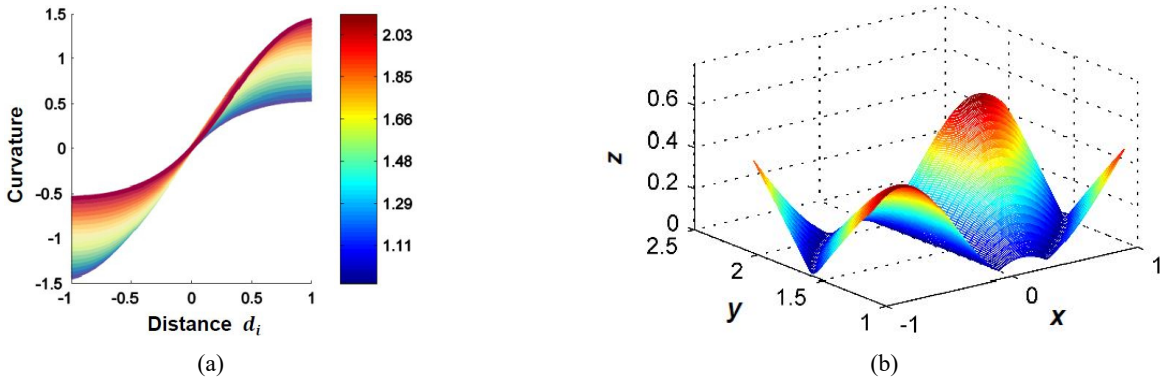

(a) (b)

Fig. 5 The relationship between calculated curvature and distance: (a) linear approximation; (b) curvature error

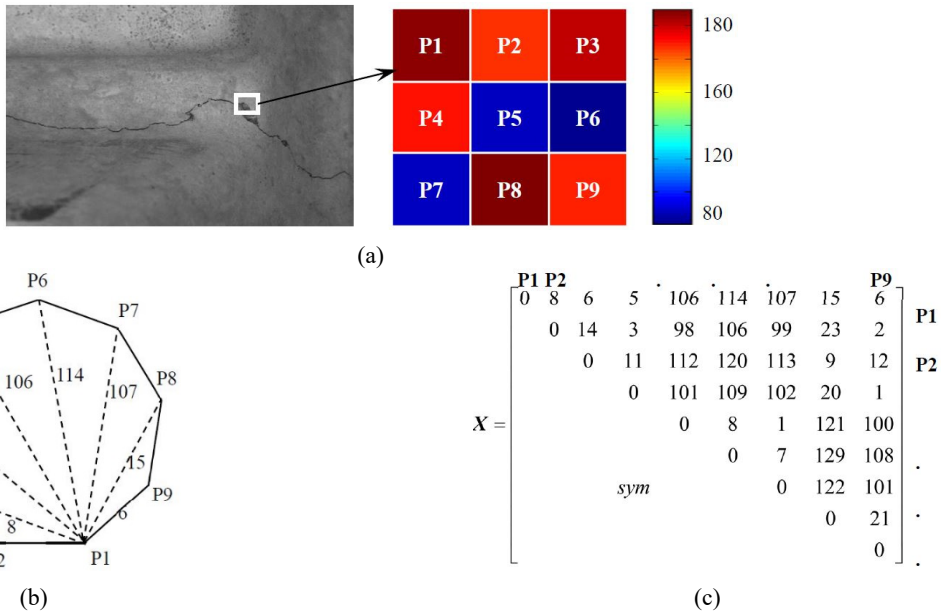

Fig. 6 Adjacency matrix establishment: (a) local pixel intensities; (b) graph illustration; (c) adjacency matrix

2.3 Graph-based anomalies calculation method

In this section, a graph-based anomalies calculation method is developed for crack identification. The applicable scope of graph-based anomalies method is extended to two-dimensional images, the specific application process is also optimized for better performance.

2.3.1 Image sub-block graph building

In general, a graph G consists of a set V of nodes and a set of links (Mirzaei and Adeli 2016), i.e., $G = \{V, E\}$, and furthermore, each link has a weight $\omega \in [0, \infty]$ representing the strength of connection. Such a graph can be represented by a symmetrical adjacency matrix $\boldsymbol{X}$ between the nodes. For a two-dimensional image, the adjacency matrix can be established as presented in Fig. 6, where the weighted between two pixels is defined as the corresponding Euclidean sequence. By this modeling, the original image can be represented by adjacency matrices

$$\boldsymbol{X} = \begin{bmatrix} \boldsymbol{X^{11}} & \boldsymbol{X^{12}} & \cdots & \boldsymbol{X^{1n}} \\ \boldsymbol{X^{21}} & \boldsymbol{X^{22}} & \cdots & \boldsymbol{X^{2n}} \\ \vdots & \vdots & & \vdots \\ \boldsymbol{X^{m1}} & \boldsymbol{X^{m2}} & \cdots & \boldsymbol{X^{mn}} \end{bmatrix} \tag{3}$$

where $\boldsymbol{X^{mn}}$ is the mn-th symmetrical adjacency matrix.

According to the definition of graphs, a graph may change its communities in the member or in the way of connections because of the cracks or texture changes. Therefore, the crack features contained in the concrete slab images of HSR may change the communities of the corresponding graphs.

2.3.2 Diagonalization and anomalies calculation

Decompose the symmetrical adjacency matrix $\boldsymbol{X^t}$ into $\boldsymbol{X^t = \Gamma \Lambda \Gamma'}$ where $\boldsymbol{\Gamma}$ is a matrix whose column is an eigenvector of $\boldsymbol{X^t}$ and $\boldsymbol{\Lambda}$ is a diagonal matrix whose contains the eigenvalues. The change of community structure can be reflected by monitoring $\boldsymbol{\Gamma}$, while the change of community activity is by $\boldsymbol{\Lambda}$. Assuming ergodicity of $\boldsymbol{X^t}$ for all the training samples (crack free samples, the number of the samples is M), the baseline can be acquired approximately as a sample mean as

$$\overline{\boldsymbol{X}} = \frac{1}{M}\sum_{t=1}^{M} \boldsymbol{X^t} \simeq \boldsymbol{\Gamma \Lambda \Gamma'} \tag{4}$$

Therefore, for a given graph, if the eigenvector $\boldsymbol{\Gamma^* \neq \Gamma}$, we consider the sub-block may have some different features (i.e., crack features).

Assuming the eigenvector $\boldsymbol{\Gamma}$ has been already estimated by decomposition of $\overline{\boldsymbol{X}}$ which is computed from the training samples, for a given $\boldsymbol{Y^t}$ we can decompose it by multiplying $\boldsymbol{\Gamma}$ and $\boldsymbol{\Gamma'}$ in both sides as

$$\boldsymbol{X^t = \Gamma Y^t \Gamma'} \tag{5}$$

Note that the obtained $\boldsymbol{Y^t}$ is not diagonal in general due to the fact that $\boldsymbol{X^t}$ cannot be kept identical to the training samples when various noises exist in real data collections. Therefore, we can separate its components into the diagonal part and the non-diagonal part as

$$\boldsymbol{X^t = \Gamma Y^t \Gamma'} = \boldsymbol{\Gamma}(diag[\boldsymbol{Y^t}])\boldsymbol{\Gamma'} + \boldsymbol{\Gamma}(non - diag[\boldsymbol{Y^t}])\boldsymbol{\Gamma'} \tag{6}$$

As the description as Eq. (6), the $diag[\boldsymbol{Y^t}]$ reflects the regular fluctuations within communities, while $non - diag[\boldsymbol{Y^t}]$ reflects the fluctuations between communities. Therefore, the $non - diag[\boldsymbol{Y^t}]$ can be regarded as the fluctuation of community structure. By the employment of Frobenius norm, the fluctuation z^t can be represented as

$$z^t = \|non - diag[\boldsymbol{Y^t}]\|_f \tag{7}$$

Algorithm 1 Pseudo code of crack identification

Required:
Collected filtered non-crack image dataset x_i;
Filtered test image y;
Threshold value λ.

1.Compute the mean adjacency matrix $\overline{\boldsymbol{X}}$ of all non-crack sub-blocks;
2.Decompose the mean adjacency matrix $\overline{\boldsymbol{X}}$ into $\overline{\boldsymbol{X}} = \boldsymbol{\Gamma\Lambda\Gamma}$'
3.**while** $t \leq$ all adjacency matrix number **do**
Compute $\boldsymbol{Y}^t$ by eigen decomposition by Eq. (5);
Separate $\boldsymbol{Y}^t$ into $diag[\boldsymbol{Y}^t]$ and $non-diag[\boldsymbol{Y}^t]$;
Compute z^t by the Frobenius form as Eq. (7);
4. Set $30 \times \bar{z}$ as the baseline;
5. Divide the filtered test image y into $m \times n$ sub-blocks;
6. $j = 0$
while $i \leq m*n$ **do**
if $z^i <$ baseline, **then** sub-block i is crack-free;
else sub-block i contain crack features, j++;
7. **if** $j > \lambda$, test image y is crack contained; **else**, it is crack-free.

2.3.3 Crack identification

To guarantee the robustness of the proposed method, a threshold is defined for the image crack detection. If the number of cracks contained sub-blocks exceeds the threshold, the image is determined as crack contained, otherwise, it is crack free. Based on the description above, the pseudo-code of the crack detection algorithm is then given in Algorithm 1.

3. Database and evaluation metrics

A finite element model is developed to represent a cracked beam element of length d and the crack is located at

3.1 Dataset

Dataset is acquired form the "2019 Artificial Intelligence and Track Safety Data Challenge" in China. The dataset samples have a resolution of 1,400 × 1,200 (pixels) and then manually labeled by some experienced inspectors for further investigation. Randomly select 100 crack-free samples (positive samples) and 100 crack samples (negative samples). To comprehensively evaluated the proposed method, acquired images are divided into two different types (obvious crack and slight crack (when the crack width is less than 6 pixels)) for experimental investigation in this section. Some typical samples of the acquired images are displayed in Fig. 7. As can be seen in Fig. 7, cracks can hardly be detected with naked eyes, especially in slight crack images. Besides, images strongly influenced by the illumination conditions and the curvature change of the concrete slabs. Some slabs are contaminated by oil stains which make it more complex for the crack contour extraction.

3.2 Evaluation metrics of accuracy

The metrics used for evaluating the final classification results mainly include precision, recall, and F1 score. Precision is the ratio of correctly predicted positive observations to the total predicted positive observations. The recall is the ratio of correctly predicted positive observations to all observations in the actual class. F1 score is the weighted average of Precision and Recall. Denoted TP as true positives (the value of the actual class is yes and the value of the predicted class is also yes), FP as false positives (actual class is no and predicted class is yes), FN as false negatives (actual class is yes but predicted class in no), the three evaluation parameters can be defined as Ma *et al*. (2016):

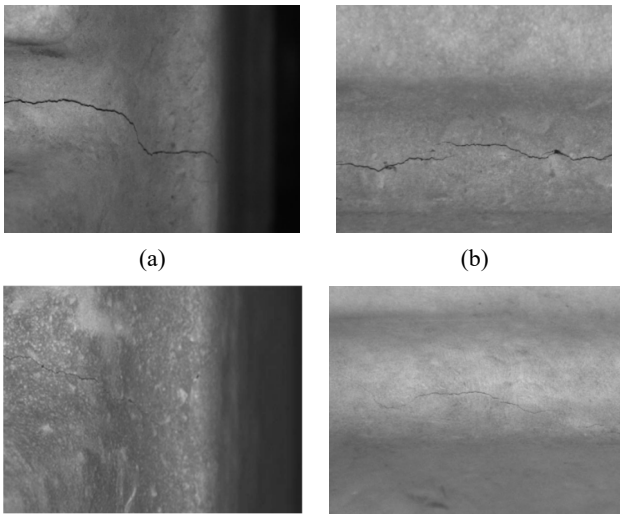

Fig. 7 Typical of images: (a)(b) obvious crack images; (c)(d) slight crack images

Precision = TP/TP + FP
Recall = TP/TP + FN
F1 Score = 2*(Recall * Precision) / (Recall + Precision)

4. Experiment

The proposed method is implemented on the Windows 10 operating system with an Intel(R) Core(TM) i5-8500 CPU. Matlab programming language is employed for the experimental coding.

4.1 Image preprocessing

In this section, Fig. 7(d) is employed for the illustration of the proposed method. After curvature filtering, the generated little curvature component is shown in Fig. 8(a). As can be seen in Fig. 8(a), little curvature contains much low-frequency trend component of the surface, While, the large curvature component of the image is filtered, as well as the crack information. Fig. 8(b) is the generated large curvature component, which contains more specific crack information and has the potential for the crack extraction. The energy evolution during the filtering process is presented in Fig. 8(c), which indicates that the regularization energy is successfully minimized (the definition of those energies can be seen in Gong and Sbalzarini (2017)). As presented in the filtering result,

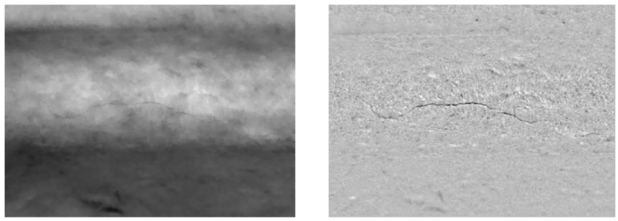

(a) (b)

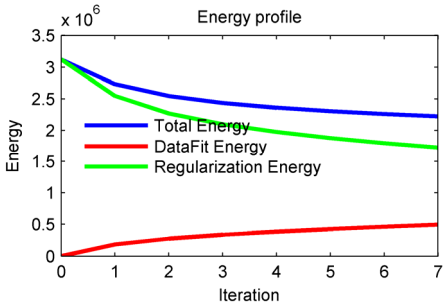

(c)

Fig. 8 Curvature filtering process: (a) large curvature component; (b) little curvature component; (c) energy evolution

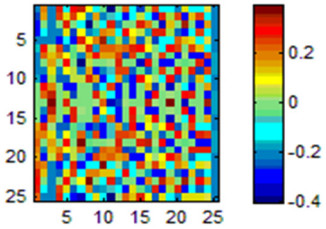

Fig. 9 Corresponding eigenvector

curvature filtering enjoys the merit of edge preservation, even when suffering the interference of complex background, illumination change, and oil pollution of the surface.

4.2 Experimental process

4.2.1 Apriori knowledge acquisition

Randomly select 100 images from the crack-free samples (positive samples)for the apriori knowledge acquisition, subdivided image blocks with 5×5 (pixels)are calculated to detect the concrete slab cracks. Accordingly, for each block, the corresponding graph can be constructed (see an illustrative example in Fig. 6). After modeling, one image is now modeled as a sequence of graphs, i.e., $F = \{G^1, G^2, \ldots G^3, \ldots\}$. Therefore, 100 images will generated 672,000 (280 × 240 × 100) graphs. Average the crack-free graph samples and diagonalize the mean graph, the generated eigenvalue can be acquired as: [-1.5812, -1.0969, -0.7843, -0.6700, -0.5039, -0.3781, -0.3397, -0.3304, -0.2309, -0.2233, -0.2219, -0.2078, -0.1823, -0.1608, -0.1551, -0.1502, -0.1422, -0.1301, -0.1264, -0.1160, -0.1111, -0.1029, -0.0976, -0.0901, 8.13325], the corresponding eigenvector is presented in Fig. 9. According to the proposed anomalies calculation, quantified fluctuation of the graph (Frobenius norm) of the images can be acquired. Setting $30 * \bar{z}$ (4.7849×10^4 in this research) as the appropriate value of baseline. If the corresponding anomaly value large than the baseline, the block might contain cracks; if the anomaly value less than the baseline, the block might be crack-free.

4.2.2 Crack identification

Divide the input image into several blocks (the block size is 5 × 5), the image will be divided into 240 × 280 block. Compute blocks by eigen decomposition according to Eq. (5) and then Separate $\boldsymbol{Y}^t$ into $diag[\boldsymbol{Y}^t]$ and $non-diag[\boldsymbol{Y}^t]$, the fluctuation z^t can be calculated. As can be seen in Fig. 10, the potential crack contained blocks are identified. In order to enhance the generalization ability of the algorithm, a threshold is employed for the determination of the image. If the number of the crack contained block is large than the threshold λ (50 in this research), the image is considered as crack contained image; if the number of the crack contained block is less than the threshold λ, the image is considered as crack free. For example, in Fig. 10, there are 53 blocks excess the threshold value. Therefore, this sample is reported as crack contained.

4.3 Results

Confusion matrix, precision, recall, and F1 score are the conventional tools for the classification algorithms. In the confusion matrix, each column of the confusion matrix represents the instances in a predicted class (output class), while each row represents the instance in an actual class (target class).

4.3.1 Obvious crack

As can be seen in Fig. 11(a), the proposed method presents a good classification ability for the obvious crack

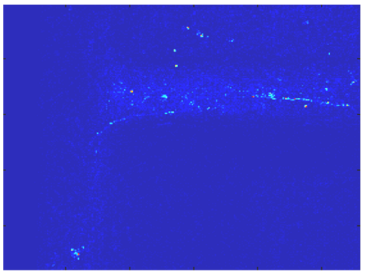

Fig. 10 Calculated graph anomalies

	C1	C2
C1	70	30
C2	0	100

(a)

	C1	C2
C1	70	30
C2	38	62

(b)

Fig. 11 Confusion matrix for the proposed method (a) Obvious crack; (b) Slight crack

Table 1 Evaluation metrics for the proposed method

Metrics	Obvious crack		Slight crack	
	C1	C2	C1	C2
Precision	0.70	1.00	0.70	0.62
Recall	1.00	0.77	0.65	0.67
F1 Score	0.82	0.87	0.67	0.64

samples, with 30 misclassifications in the entire 200 testing records. Therefore, the accuracy rate of the proposed method is calculated at 85.00%. The calculated evaluation metrics of two conditions (C1 indicates the crack-free samples, C2 indicates the obvious crack samples) are shown in Table 1. The acquired mean precision, recall, and F1 are calculated to be 0.85, 0.89, and 0.85 respectively. The results validate the effectiveness of the proposed method in obvious crack samples.

4.3.2 Slight crack

As can be seen in Fig. 11(b), the proposed method reported a poor result for the slight crack samples compared with obvious samples, with 68 misclassifications in the entire 200 testing records. Therefore, the accuracy rate of the proposed method is calculated at 66.00%. A possible explanation is that the subtle gradations generated in the slight crack image make it hard to identify. The results evaluation effects of two conditions (C1 indicates the crack-free samples, C2 indicates the slight crack samples) are shown in Table 1. The acquired mean precision, recall, and F1 are calculated to be 0.66, 0.66, and 0.64 respectively. The results also validate the effectiveness of the proposed method in slight crack samples.

5. Discussion

5.1 Comparative analysis of different edge detectors

Basic image processing techniques, such as edge and boundary detection, are intensively used in crack detection. To further investigate the crack identification ability with different edge detectors, series experiments are conducted. The acquired image and its corresponding edge maps obtained by different edge detectors and the proposed curvature-based method are shown in Fig. 12. The results for some traditional edges detectors, i.e., Canny (Fig. 10(c)), Sobel (Fig. 12(d)), Prewitt (Fig. 12(e)), Roberts (Fig. 12(f)), show that these detectors are very sensitive to the noise (caused by the illumination and imaging process) and background profile (caused by the complex concrete slab surfaces) interferences. Different from the traditional edge detectors, the curvature filtering method offers an extraordinary crack edge preservation ability (Fig. 12(b)), even when suffering the interference of complex background, illumination change, and oil pollution of the surface. The classification results are shown in Table 2. The results show that very little information is available for the crack information. The reported mean classification accuracy rate for different edge detectors (Canny, Sobel Prewitt, Roberts) is calculated to be 0.5, 0.5, 0.5, and 0.5 respectively. Furthermore, we have noticed, most surprisingly, that all the samples are identify into same class (either C1 or C2). The results show that binary edge information provides few crack information and cannot be directly used for crack identification via the proposed method.

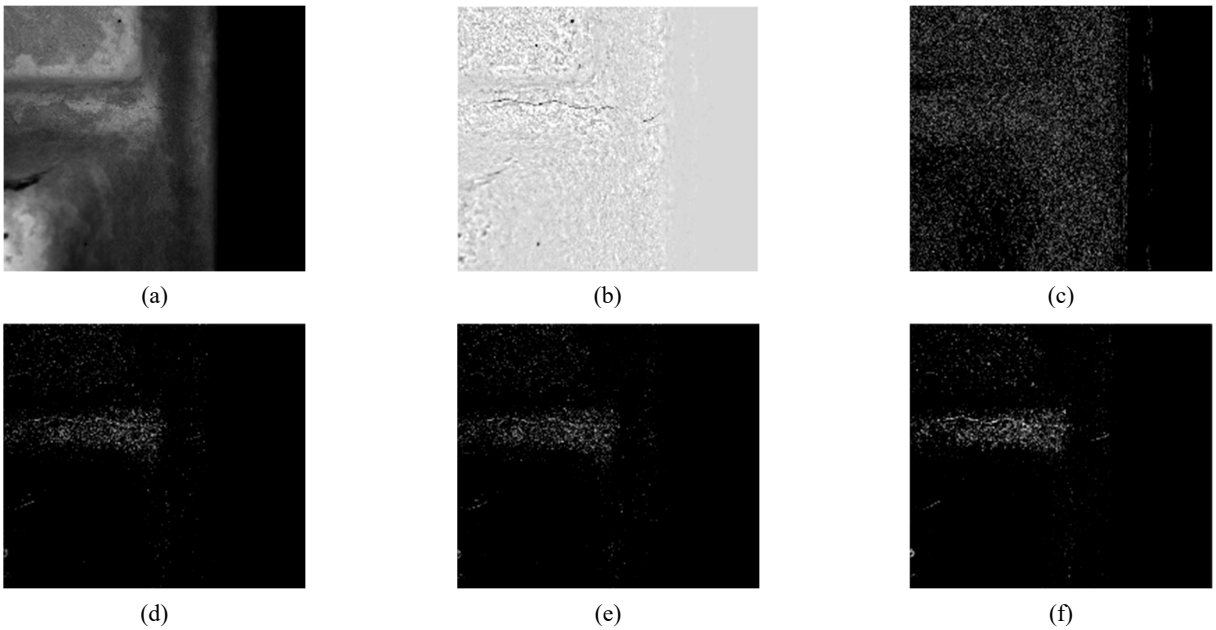

Fig. 12 Extracted edge maps for different methods (a) original image; (b) proposed method; (c) Canny; (d) Sobel; (e) Prewitt; (f) Roberts

Table 2 Accuracy for different edge detectors

Edge detector	Obvious crack	Slight crack
Canny	0.50	0.50
Sobel	0.50	0.50
Prewitt	0.50	0.50
Roberts	0.50	0.50

5.2 Comparative analysis with machine learning techniques

To further evaluate the proposed method, the results are compared with two different machine learning techniques (MLs, CNN and ResNet). Acquired images are divided into two different types (crack and crack-free) for experimental investigation in this experiment. The employed CNN model is described in Sun *et al*. (2017); the chosen ResNet is described in Ou *et al*. (2019). In order to deeply investigate the influence of the number of training samples, the original dataset (200 samples) is extended to 1000 (500 positive samples and 500 negative samples). The machine learning techniques are implemented on the Linux operating system with Intel (R) Core (TM) i7-8700 CPU @ 3.20 GHz and NVIDIA GeForce RTX 2070 GPU. Python programming language is employed for the experimental coding.

The classification results in different machine learning techniques are shown in Table 3. Crack detection in different methods is also presented in Fig. 13. As can be seen in Fig. 13(c), the CNN method seems successfully capture the crack features in obvious crack samples. However, it is still a significant challenge to acquire the

Table 3 Evaluation metrics for different machine learning techniques

MLs	Metrics	Obvious crack		Slight crack	
		C1	C2	C1	C2
CNN (200 samples)	Precision	0.45	0	0	0.55
	Recall	1	0	0	1
	F1 Score	0.62	0	0	0.71
CNN (1000 samples)	Precision	0.49	0	0.49	0
	Recall	1	0	1	0
	F1 Score	0.66	0	0.66	0
ResNet (200 samples)	Precision	0.94	0.95	0.45	0
	Recall	0.94	0.95	1	0
	F1 Score	0.94	0.95	0.62	0
ResNet (1000 samples)	Precision	1	1	0.49	0
	Recall	1	1	1	0
	F1 Score	1	1	0.66	0

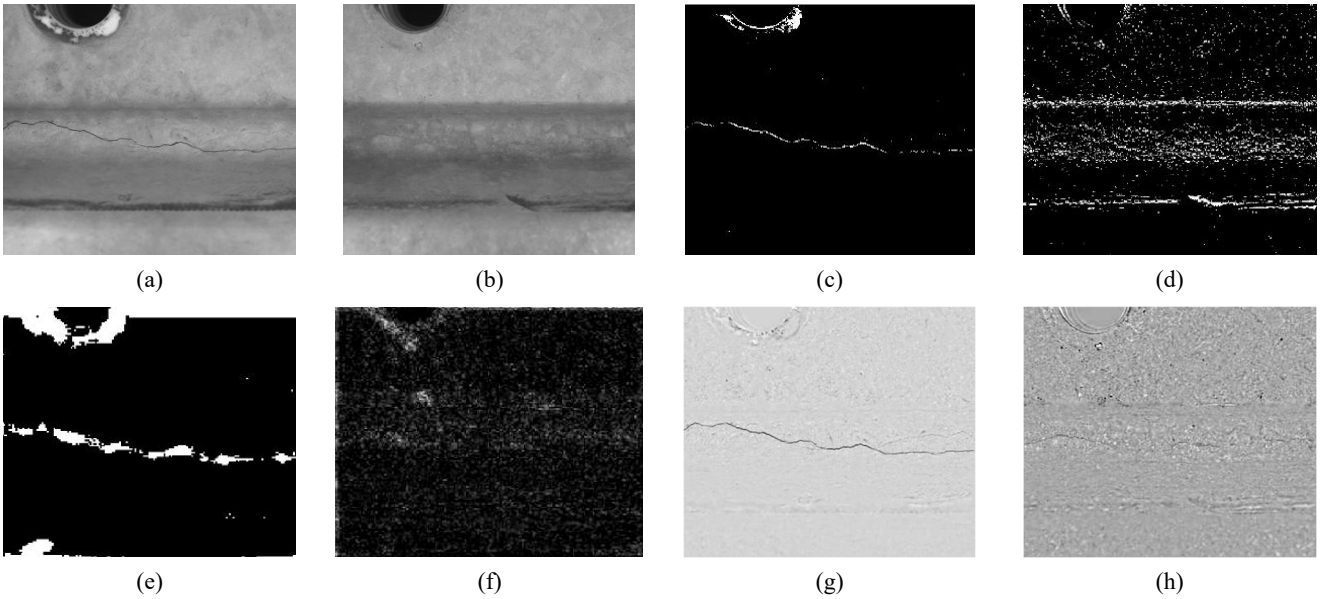

(a) (b) (c) (d)

(e) (f) (g) (h)

Fig. 13 Crack detection in different methods: (a)(b) typical obvious and slight crack samples; (c)(d) deep layer features of CNN method; (e)(f) deep layer features of ResNet method; (e)(f) detection result of the proposed method

crack information in slight crack samples (Fig. 13(d)). As listed in Table 3, CNN reports a poor classification ability (nearly 50% in both 200 samples and 1000 samples) no matter how many samples are contained in the dataset. As shown in Fig. 14(e), ResNet reports a positive effect in obvious crack samples. Nevertheless, in slight crack samples, the characteristics of cracks seem strongly affected by the noise and hard to be identified. The superiority of ResNet is fully reflected according to Table 3. When the number of the samples is 200, the mean F1 score is reported as 0.95 (obvious crack). When the number of the samples extended to 1000, the mean F1 score for ResNet can be calculated as 1 (obvious crack). The performance of ResNet, however, is still limited for the slight crack situation, as well as CNN. A possible explanation is that the slight crack information might be neglected by the pooling layers contained in the network (whether in CNN or ResNet). The comparative experiment leads us to conclude that machine learning techniques might be influenced by the size of the training set. On the basis of our findings, it can be concluded that the crack identification ability is largely influenced by the choice of machine learning techniques. The extracted crack features based on the proposed method are shown in Figs. 13(g) and (h). It seems the proposed method successfully foregrounds the crack characteristic whether in the obvious and slight crack situation.

6. Conclusions

This paper introduces a zero-shot crack detection method is proposed for the state monitoring of concrete slabs of high-speed railway via graph-based anomalies calculation. Combined with curvature filtering and graph-based anomalies calculation, the sub-blocks with cracks are successfully identified. The behavior of the proposed large curvature information extraction approach makes us conclude that this approach performs considerably well in crack feature extraction even under different curvature structures and illumination conditions. The graph-based anomalies method has proved very useful for sub-block crack identification. Various noise interferences are taking into account by the graph-based model which means better robustness in real application scenarios. The proposed graph-based non-contact fatigue crack detection method would have more hopeful prospects in other infrastructure systems detection. The large curvature information extraction approach can be used to enhance the defects information, and the graph-based anomalies method is implemented to locate the defects. Compared with other detection methods, the proposed method can recognize the crack samples with few or even no training samples. In summary, these findings reveal an important new strategy for infrastructure cracks detection.

Although the proposed method performs well in the crack detection of concrete slabs, the applicability of the method is still limited by the calculation efficiency. As a decisive factor for real-time crack detection, rapid detection is crucial for the health monitoring of HSR. However, in this research, the proposed method would take about fifteen seconds for an image to identify the cracks. Future work will focus on calculation efficiency improvement, automatic threshold optimization, and extending this work toward more application scenarios.

Acknowledgments

The research described in this paper was financially supported by the Zhejiang Provincial Natural Science Foundation of China (Nos. LQ21E050003 and LQ20E050027), the Zhejiang Special Support Program for High-level Personnel Recruitment of China (No. 2018R52034), the National Natural Science Foundation of China (No. U1909217), and the Fundamental Scientific Research Project of Wenzhou (No. G20190013).

References

Ahmadlou, M. and Adeli, H. (2012), "Visibility graph similarity: A new measure of generalized synchronization in coupled dynamic systems", *Physica D*: *Nonlinear Phenom*., **241**(4), 326-332. https://doi.org/0.1016/j.physd.2011.09.008

Ahmadlou, M. and Adeli, H. (2017), "Complexity of weighted graph: A new technique to investigate structural complexity of brain activities with applications to aging and autism", *Neurosci*. *Lett*., **650**, 103-108. https://doi.org/10.1016/j.neulet.2017.04.009

Ai, C., Qiu, S., Zhang, A. and Wang, K.C.P. (2018), "A nonballasted rail track slab crack identification method using a level-set-based active contour model", *Comput*.*-Aid*. *Civil Infrastr*. *Eng*., **33**, 571-584. https://doi.org/10.1111/mice.12362

Bang, S., Park, S., Kim, H. and Kim, H. (2019), "Encoder-decoder network for pixel-level road crack detection in black-box images", *Comput*.*-Aid*. *Civil Infrastr*. *Eng*., **34**, 713-727. https://doi.org/10.1111/mice.12440

Bayar, G. and Bilir, T. (2019), "A novel study for the estimation of crack propagation in concrete using machine learning algorithms", *Constr*. *Build*. *Mater*., **215**, 670-685. https://doi.org/10.1016/j.conbuildmat.2019.04.227

Bilge, H., Doruk, E., Findik, F. and Pakdil, M. (2019), "Effect of fatigue crack propagation on natural frequencies of system in AISI 4140 Steel", *Steel Compos*. *Struct*., *Int*. *J*., **32**(3), 305-312. https://doi.org/10.12989/scs.2019.32.3.305

Cha, Y., Choi, W., Suh, G. and Mahmoudkhani, S. (2018), "Autonomous structural visual inspection using region-based deep learning for detecting multiple damage types", *Comput*.*-Aid*. *Civil Infrastr*. *Eng*., **33**(9), 731-747. https://doi.org/10.1111/mice.12334

Colla, C., Krause, M., Maierhofer, C., HoÈhberger, H.-J. and Sommer, H. (2002), "Combination of NDT techniques for site investigation of non-ballasted railway tracks", *NDT E Int*., **35**, 95-105. https://doi.org/10.1016/S0963-8695(01)00033-0

Fan, H., Cosman, P.C., Hou, Y. and Li, B. (2018), "High-speed railway fastener detection based on a line local binary pattern", *IEEE Signal Process*. *Lett*., **25**(6), 788-792. https://doi.org/10.1109/LSP.2018.2825947

Gong, Y. and Sbalzarini, I.F. (2017), "Curvature Filters Efficiently Reduce Certain Variational Energies", *IEEE Transact*. *Image Process*., **26**(4), 1786-1798. https://doi.org/10.1109/TIP.2017.2658954

Kang, M.S., An, Y.K. and Kim, D.J. (2018), "Electrical impedance-based crack detection of SFRC under varying environmental conditions", *Smart Struct*. *Syst*., *Int*. *J*., **22**(1), 1-11. https://doi.org/10.12989/sss.2018.22.1.001

Kong, X. and Li, J. (2019), "Non-contact fatigue crack detection

in civil infrastructure through image overlapping and crack breathing sensing", *Automat. Constr.*, **99**, 125-139. https://doi.org/10.1016/j.autcon.2018.12.011

Leaman, F., Herz, A, Brinnel, V., Baltes, R. and Clausen, E. (2020), "Analysis of acoustic emission signals during fatigue testing of a M36 bolt using the Hilbert-Huang spectrum", *Struct. Monitor. Maint., Int. J.*, **7**(1), 13-25. https://doi.org/10.12989/smm.2020.7.1.013

Li, H., Strauss, J. and Lu, L. (2019), "The impact of high-speed rail on civil aviation in China", *Transport Policy*, **74**, 187-200. https://doi.org/10.1016/j.tranpol.2018.11.015

Liu, Z., Cao, Y., Wang, Y. and Wang, W. (2019), "Computer vision-based concrete crack detection using U-net fully convolutional networks", *Automat. Constr.*, **104**, 129-139. https://doi.org/10.1016/j.autcon.2019.04.005

Lu, G., Liu, J. and Yan, P. (2018), "Graph-based structural change detection for rotating machinery monitoring", *Mech. Syst. Signal Process.*, **99**, 73-82. https://doi.org/10.1016/j.ymssp.2017.06.003

Luo, L., Feng, M.Q., Wu, J. and Leung, R.Y. (2019), "Autonomous pothole detection using deep region-based convolutional neural network with cloud computing", *Smart Struct. Syst., Int. J.*, **24**(6), 745-757. https://doi.org/10.12989/sss.2019.24.6.745

Ma, J., Sun, L., Wang, H., Zhang, Y. and Aickelin, U. (2016), "Supervised anomaly detection in uncertain pseudoperiodic data streams", *ACM Transact. Internet Technol.*, **16**(1), 1-20. https://doi.org/10.1145/2806890

Maeda, K., Takahashi, S., Ogawa, T. and Haseyama, M. (2019), "Convolutional sparse coding-based deep random vector functional link network for distress classification of road structures", *Comput.-Aid. Civil Infrastr. Eng.*, **34**, 654-676. https://doi.org/10.1111/mice.12451

Mirzaei, G. and Adeli, H. (2016), "Resting state functional magnetic resonance imaging processing techniques in stroke studies", *Rev. Neurosci.*, **27**(8), 871-885. https://doi.org/10.1515/revneuro-2016-0052

Nayyeri, F., Hou, L., Zhou, J. and Guan, H. (2019), "Foreground-background separation technique for crack detection", *Comput.-Aid. Civil Infrastr. Eng.*, **34**, 457-470. https://doi.org/10.1111/mice.12428

Ou, X. Yan, P., Zhang Y., Tu, B., Zhang G., Wu, J. and Li, W. (2019), "Moving object detection method via ResNet-18 with encoder–decoder structure in complex scenes", *IEEE Access*, **7**, 108152-108160. https://doi.org/10.1109/ACCESS.2019. 2931922

Ozcan, G., Kocak, Y. and Gulbandilar, E. (2017), "Estimation of compressive strength of BFS and WTRP blended cement mortars with machine learning models", *Comput. Concrete, Int. J.*, **19**(3), 275-282. https://doi.org/10.12989/cac.2017.19.3.275

Sanchez, M., Atique, A., Kim, S., Romero, E. and Zielinski, M. (2013), "Exploring desiccation cracks in soils using a 2D profile laser device", *Acta Geotechnica*, **8**, 583-596. https://doi.org/10.1007/s11440-013-0272-1

Song, S.P. and Ni, Y.J. (2018), "Ultrasound Imaging of Pipeline Crack Based on Composite Transducer Array", *Chinese J. Mech. Eng.*, **31**, 1-10. https://doi.org/10.1186/s10033-018-0280-z

Sun, W., Yao, B., Zeng, N., Chen, B., He, Y., Cao, X. and He, W. (2017), "An intelligent gear fault diagnosis methodology using a complex wavelet enhanced convolutional neural network", *Materials*, **10**(7), 1-18. https://doi.org/10.3390/ma10070790

Sun, W., Zhou, Y., Cao, X., Chen, B., Feng, W. and Chen, L. (2020), "A two-stage method for bearing fault detection using graph similarity evaluation", *Measurement*, **165**, 108-138. https://doi.org/10.1016/j.measurement.2020.108138

Wang, C., Zhou, S., Wang, B., Guo, P. and Su, H. (2016), "Settlement behavior and controlling effectiveness of two types of rigid pile structure embankments in high-speed railways", *Geomech. Eng., Int. J.*, **11**(6), 847-865. https://doi.org/10.12989/gae.2016.11.6.841

Wang, W., Zhang, A., Wang, K.C.P., Braham, A.F. and Qiu, S. (2018), "Pavement crack width measurement based on Laplace's equation for continuity and unambiguity", *Comput.-Aid. Civil Infrastr. Eng.*, **33**, 110-123. https://doi.org/10.1111/mice.12319

Wang, T., Lu, G. and Yan, P. (2020), "A Novel Statistical Time-Frequency Analysis for Rotating Machine Condition Monitoring", *IEEE Transact. Indust. Electron.*, **67**(1), 531-541. https://doi.org/10.1109/TIE.2019.2896109

Woo, S. and Yeo, H. (2016), "Optimization of pavement inspection schedule with traffic demand prediction", *Procedia – Soc. Behav. Sci.*, **218**, 95-103. https://doi.org/10.1016/j.sbspro.2016.04.013

Xi, P., Ye, X., Jin, T. and Chen, B. (2018), "Structural performance monitoring of an urban footbridge", *Struct. Monitor. Maint., Int. J.*, **5**(1), 129-150. https://doi.org/10.12989/smm.2018.5.1.129

Xiang, J., Nackenhorst, U., Wang, Y., Jiang, Y., Gao, H. and He, Y. (2014), "A new method to detect cracks in plate-like structures with though-thickness cracks", *Smart Struct. Syst., Int. J.*, **14**(3), 397-418. https://doi.org/10.12989/sss.2014.14.3.397

Ye, X., Jin, T. and Yun, C. (2019), "A review on deep learning-based structural health monitoring of civil infrastructures", *Smart Struct. Syst., Int. J.*, **24**(5), 567-585. https://doi.org/10.12989/sss.2019.24.5.567

Zhang, A., Wang, K.C.P., Fei, Y., Liu, Y., Chen, C., Yang, G. and Yang, E. (2019), "Automated Pixel-Level Pavement Crack Detection on 3D Asphalt Surfaces with a Recurrent Neural Network", *Comput.-Aid. Civil Infrastr. Eng.*, **34**, 213-229. https://doi.org/10.1111/mice.12409

Zhuang, L., Wang, L., Zhang, Z. and Tsui, K.L. (2018), "Automated vision inspection of rail surface cracks : A double-layer", *Transport. Res. Part C: Emerg. Technol.*, **92**, 258-277. https://doi.org/10.1016/j.trc.2018.05.007

CC